

# Measurement of Effective Magnetic Permeability of Soft Magnetic Materials using Electrical Impedance Spectroscopy



Alexandru Okos<sup>1\*</sup>, Robert Radu Piticescu<sup>1\*</sup>, Cristian Bogdanescu<sup>1</sup>, Paul Stanciu<sup>1</sup>, Vasile Somoghi<sup>2</sup> and Marcel Istrate<sup>2</sup>

<sup>1</sup>National Research and Development Institute for Non-ferrous and Rare Metals, Romania

<sup>2</sup>S C STIMPEX S.A. Bucharest, Romania

Submitted: August 21, 2023; Published: September 12, 2023

\*Corresponding author: Alexandru Okos and Robert Radu Piticescu, National Research and Development Institute for Non-ferrous and Rare Metals, Romania Email: alexandru.okos@imnr.ro, rpiticescu@imnr.ro

## Abstract

Soft magnetic materials are important components of electronic devices. Knowledge of the exact magnetic properties of these materials is essential for the design of devices that utilize them. We tested the possibility of measuring the inductance factor ( $Al$ ), static effective permeability ( $\mu_{eff}$ ) and static initial permeability ( $\mu_i$ ), complex permeability ( $\mu'$  and  $\mu''$ ) of a ferrite core using electrical impedance spectroscopy (EIS).  $B(H)$  hysteresis curves were also recorded using the same setup. This allowed the estimation of the values for the coercive field ( $H_C$ ) and for the saturation magnetic polarization ( $B_i$ ). The material selected for the test is 3F3 and the type of the core used is P26/16. The results obtained from our measurements are of the same order of magnitude as the magnetic properties specified by the manufacturer.

**Keywords:** Complex magnetic permeability; Ferrite cores; Impedance spectroscopy

## Introduction

Magnetic materials can be divided into two classes according to their properties: hard magnetic materials and soft magnetic materials. The hard magnetic materials are permanent magnets. They are characterized by high remanence, high coercive fields and large hysteresis loops. Soft magnetic materials are characterized by low remanence, low coercive fields and narrow hysteresis loops. The energy losses in a magnetic material are proportional to the area of the hysteresis curve. Therefore, soft magnetic materials are found in applications where fast switching of magnetization is required. Usually, these are magnetic cores of various inductors, high frequency noise filters, transformers, antennas and actuators [1-3]. The properties of magnetic materials are specified by the manufacturer along with the measurement conditions. Nevertheless, recreating the same measurement conditions is not at all times straight forward and complicated experimental setups could be required depending on the parameter that is investigated and the sought accuracy of the results. Investigation equipment range from LCR meters to vibrating sample - superconducting quantum interference device magnetometers (SQUID-VSM) [4-6]. The easiest method to determine the magnetic permeability of a

material is to prepare an inductor based on the respective material and analyse the electrical response of the inductor using an oscilloscope and a function generator [4]. In this paper we explore the possibility of extending the analysis capabilities of electrical impedance spectroscopy (EIS) instruments to the study of magnetic properties. EIS devices are designed to measure the electric properties of electrochemical cells. Such cells are highly non-linear. Therefore, EIS machines typically output very small voltages so that, on the tested voltage range, the behaviour of the electrochemical cell can be considered linear. This limits the strength of the magnetic field generated by an inductor measured during an EIS experiment. The limitation in field strength could influence the accuracy of measurements [4]. One alternative to high currents is increasing the number of windings in the coil. By increasing the number of windings, the parasitic capacitance of the coil is also increased [2]. The increase of the capacitance limits the measurements to relatively low frequencies. In this study EIS was used for determining the complex effective relative magnetic permeability and the magnetic hysteresis curve of a ferrite material. The material was available as a pot type core. An inductor consisting of a

single coil was wound on the respective core. The magnetic characteristics of the core material were calculated based on the impedance response of the inductor. To the best of our knowledge this potential application for EIS has been little studied, primarily due to the ill suitability of EIS machines to drive coils and due to the availability of better suited alternatives. Yabukami et al. [7] used EIS for the determination of magnetic permeability of CoNbZr thin films at frequency ranges from 100 MHz up to several GHz. The method proposed by Yabukami is ingenious because it determines the magnetic properties based on electrical impedance variations caused by the skin effect inside the magnetic film (similarly to the working principle of a giant magnetoimpedance device). This requires an electrically conductive sample. The material examined in our study is an electrical insulator, therefore the method was not available for our case. Denk and Hofbauer [8] used an inventive two-coil setup, similar to Helmholtz coils, to investigate the magnetic properties of materials. The authors measured the static magnetic permeability of various ferromagnetic materials by using the property of ferromagnets to concentrate the magnetic field lines. They showed that it is possible to calculate the relative permeability of the test material by probing the magnetic field between the two coils, with, and without the presence of a sample. The method described by [8] is very well suited for investigating bulk samples, under DC (and even AC) conditions, however it is again not accessible for our case due to core geometry restrictions. Typically, a two-coil system used for determining the B(H) hysteresis

curves of a material [8]. In the two-coil configuration one coil is used to generate a magnetic field (H) and the other coil is used for measuring the resulting magnetic flux, and consequently the flux density (B), through the sample. However, it is possible to use a single coil simultaneously for both roles (generator and analyzer).

### Materials and Methods

The material selected for the experiments is the 3F3 ferrite. Pot type cores of the P26/16 size code constructed from 3F3 were purchased from Ferroxcube. The core was loaded with a homemade coil. The coil consists of 60 turns of 0.3 mm diameter enamel Cu wire. EIS spectra were recorded using a Metrohm Autolab PGSTAT128N instrument equipped with a FRA32M frequency response analyser module. The device was configured in a two-electrode mode with the working electrode (WE) and the sensing electrode (S) connected to each other and then to one coil terminal respectively the counter electrode (CE) and reference electrode (RE) connected to each other and to the opposite coil terminal. Figure 1 shows the image and the connection diagram of the setup. Measurements were carried out using both galvanostatic and potentiostatic configurations with applied currents between 0.5 mA and 7 mA, in the frequency range of 0.1 Hz – 50 kHz. All measurements were carried out in air at room temperature. The clamping force on the core was not measured. Data were analyzed and fitted using the Nova 2.1 software.

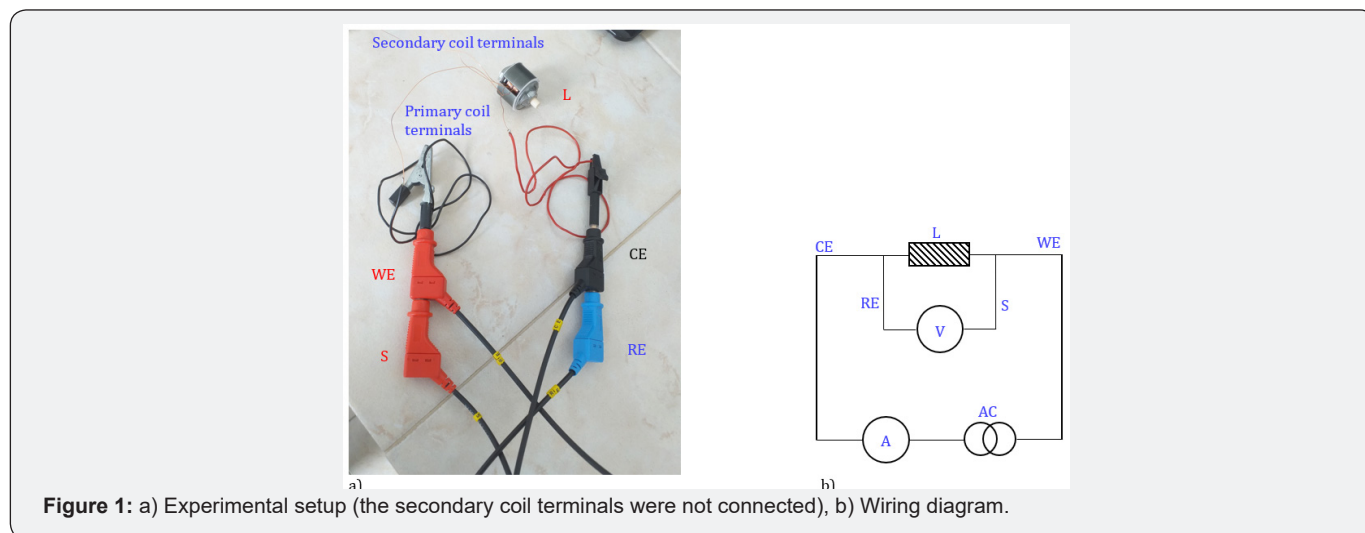


Figure 1: a) Experimental setup (the secondary coil terminals were not connected), b) Wiring diagram.

The objective of this work is to verify the relative effective permeability of a soft magnetic material by electrical impedance measurements. The relative magnetic permeability is a complex number, defined according to equation (1) where  $j$  is the imaginary unit. Permeability has a real part ( $\mu'$ ) and an imaginary part ( $\mu''$ ). The real part describes the lossless magnetization processes. The imaginary part describes the energy losses within the materi-

al as the magnetic moments lag behind the direction of an applied alternating H field. Both components of permeability typically depend on the intensity of the applied alternating magnetic field H, the intensity of a superimposed constant magnetic field, AC frequency, reluctance, temperature, pressure [9-11].

$$\mu_r = \mu'_r - j\mu''_r \quad (1)$$

Impedance is also a complex number, commonly expressed by equation (2), where  $j$  represents the imaginary unit.

$$Z = \text{Re} - j\text{Im} = Z' - jZ'' \quad (2)$$

The real part of the impedance relates to the ohmic resistance of the circuit and constitutes energy dissipation. The imaginary part of the impedance relates to the reactance of the circuit and characterizes the ability of the reactive circuit element to store energy. Reactance can be capacitive or inductive and induces a phase shift between the applied voltage on the terminals of a circuit element and the ensuing current. For an ideal inductor the impedance contains only the inductive reactance and the current lags behind the voltage by a phase shift of  $\pi/2$  radians. The inductive reactance ( $X_L$ ) depends on the signal frequency ( $f$ ) and on the inductance of the coil ( $L$ ) according to equation (3), where  $\omega$  is the angular frequency.

$$X_L = j\omega L = j2\pi fL \quad (3)$$

The inductance ( $L$ ) depends on the geometric dimensions of the coil, on the number of turns and on the relative magnetic permeability of the core according to (4), where  $N$  is the number of turns,  $S$  is the cross-sectional area of the magnetic circuit,  $l$  is the length of the magnetic circuit and  $\mu_0$  is the magnetic permeability of vacuum.

$$L = \frac{N^2 S \mu_0 \mu_r}{l} \quad (4)$$

If it can be assumed that  $\mu_r$  from equation (4) can be formal-

ly replaced by the complex permeability from equation (1) then the impedance of a non-ideal inductor can be written as shown in equation (5) where  $R_L$  represents the ohmic resistance of the inductor.

$$Z = R_L - \frac{N^2 S \omega \mu_0 \mu_r''}{l} - \frac{N^2 S \omega \mu_0 \mu_r'}{l} j \quad (5)$$

Then it follows by matching the terms that the imaginary part of the impedance contains the lossless component of the complex relative permeability. The real part of the impedance contains two terms describing losses in the system. These are the ohmic resistance of the coil ( $R_L$ ) and the magnetic losses (described by  $\mu''$ ). Therefore, the equations relating the real and imaginary parts of the complex relative magnetic permeability to the real and imaginary parts of the impedance are:

$$\mu_r' = \frac{Z'' l}{N^2 S \omega \mu_0} \quad (6)$$

$$\mu_r'' = \frac{(R_L - Z') l}{N^2 S \omega \mu_0} \quad (7)$$

It is apparent that the physical interpretation of defining the relative magnetic permeability as a complex number is adding a virtual resistor in series with an ideal inductor. This resistor is then a model for the core losses of the material. The situation is symmetrical to the case of the electric permittivity of a material, where the interpretation of defining the relative permittivity as a complex number is adding a virtual resistor in parallel to the ideal capacitor. Then the parallel resistor models the dielectric losses of the material.

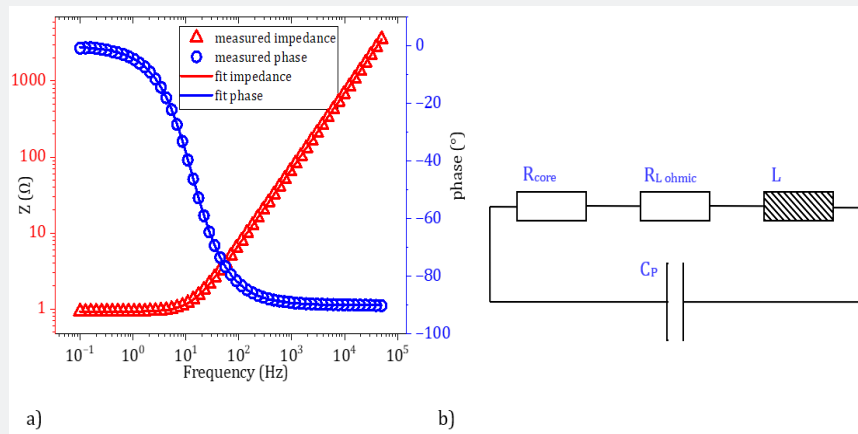


**Figure 2:** a) Impedance modulus (red) and phase (blue) measured for the inductor sample. Experimental data is shown by points. Solid lines show the fit curves. b) Circuit used for fitting EIS data.  $R_{core}$  represents the core losses,  $R_L$  represents the ohmic resistance of the coil when no core is present,  $L$  represents the inductance of the coil and  $C_p$  represents the parasitic capacitance of the windings.

We verified two paths for determining the magnetic permeability of the material from the electrical impedance of an inductor. These methods are

- i) fitting the experimental Bode plots
- ii) directly extracting material properties from the impedance measurements.

For the fitting experiment, the FRA32M module was set up to inject a current of constant amplitude through the inductor. The measured parameters are the voltage drop across the inductor terminals and the sampling time. The equipment then automatically calculates the impedance modulus and the impedance phase. From the modulus and the phase values, the real and imaginary components of the impedance are extracted. Figure 2 shows the experimental results and the circuit used for the fit of the Bode diagrams for modulus and phase.

From equation (4) it can be observed that in order to obtain an estimation of the relative effective permeability, as a constant real

value, independent of frequency, it is sufficient to determine the inductance of the coil. The inductance value is obtained by fitting the measured impedance data. In the circuit shown in figure 2b the inductance of the sample is modelled as an ideal inductor connected in series with two resistors and in parallel with a capacitor.  $R_L$  represents the ohmic resistance of the Cu wire. The value of  $R_L$  was measured under DC without the presence of the core and was fixed during the fitting procedure.  $R_{core}$  represents the core losses. CP represents the sum of the parasitic capacitances from the coil itself, the cables used for the connections and the internal capacity of the instrument. The results of the fit are shown in table 1. The inductance of the coil was consequently determined to be 11.1 mH. The fitting algorithm employed by the Nova software indicates a good fit when the  $\chi^2$  figure of merit approaches 0. With this circuit  $\chi^2$  was observed to decrease to 0.000835. It should be noted that the error in the estimation of C is 22%. The effect of the parasitic capacitance is observed to be negligible in the frequency range of this test.

**Table 1:** Results of the fit.

Element	Value	Unit	Estimated Error (%)
$R_{core}$	$5.1 \times 10^{-3}$	$\Omega$	15.6
$C_p$	$1.34 \times 10^{-11}$	F	22.2
$R_L$	0.919	$\Omega$	fixed
L	0.011108	H	0,071
g.o.f. ( $\chi^2$ )	0.000835	-	-

**Table 2:** Values of material characteristics.

Property / Dimension	Unit	Specified	Manufacturing Tolerance	Measured / Deduced	Relative Error
Air gap	mm	$\approx 0$	-	$6.7 \times 10^{-3} *$	-
$\mu_i$	adim.	2000	+/- 20%	$\approx 1200$	40%
$\mu_{eff}$	adim.	1470	-	$\approx 982$	33%
Al	nH/turn	4600	+/- 25%	$\approx 3100$	32%

\*deduced from  $\mu_i$  and  $\mu_{eff}$  values specified by the producer.

The relative effective permeability ( $\mu_{eff}$ ), the relative initial permeability ( $\mu_i$ ) and the induction factor (Al) were calculated from the inductance value returned by the fit. The relative initial permeability is the relative permeability of the material at low magnetic H fields. The relative effective permeability takes into account the presence of an air gap in the circuit. The induction factor relates the induction of the coil to the number of turns. Table 2 compares the results available in literature for the 3F3 material [10] to the values measured during our experiment. Since both  $\mu_i$  and  $\mu_{eff}$  are provided by the manufacturer [10,11] these values were used to estimate the intrinsic air gap.

For low frequencies ( $f < 100$  kHz) core losses are specified as nearly 0 [11]. Due to the limitations of the spectrometer the mea-

surements had to be conducted at frequencies less than 50 kHz. Accurate determination of the imaginary part of the permeability for 3F3 is therefore not feasible using our EIS machine. For the experimentally determined parameters it is observed that the obtained values are different from the expected values by as much as 40%. There are a few tentative explanations why this is the case. Firstly, the values defined by the producer are already reported with relatively high tolerances (20% to 25%) therefore differences between theoretical and measured values could be expected. Secondly, the value of the air gap has a significant influence on the permeability value of a material. Ideally the measurement should be performed on a toroidal core so that the entire magnetic flux is contained within the material. The P26/16 core is a pot type core

and the alignment of the two halves of the core was never perfect. Misalignment could lead to the formation of an air gap of unknown dimensions and could cause stray flux and flux fringing effects. Another reason is the fact that the measurement conditions defined by the manufacturer are not exactly reproduced. The 3F3 material is magnetoelastic. Pressure applied to the material alters its magnetic characteristics. The published values are obtained under a clamping force of 200 +/- 50 N. Our measurements were performed without any substantial clamping. Finally, the initial permeability is not rigorously defined for 3F3. The value is defined as measured using a very low field strength [11] but the actual numerical value of the H field is not provided. Our measurements were carried out using a current of 0.5 mA which should generate under those conditions (60 turns, P26/16 core) a field of 0.8 A/m which might be too low to produce observable results. For perspective, absolute saturation of the core appears at 1200 A/m and technical saturation is achieved at 250 A/m.

For the 3f3 material  $\mu'$  is constant up to 400 kHz [10] and  $\mu''$

is less than 20 up to 200 kHz [10]. We tested the material up to 50kHz. Due to the low frequency the magnetic permeability of the material can be approximated as a real constant value. On these conditions a simple fit of the experimental data can return an estimate of the magnetic permeability. For a general case, the Bode plot fit approach has some obvious limitations. It attempts to fit the experimental data by modelling the sample with an electrical circuit and finding the macroscopic values of the circuit elements (here resistances, capacities and inductances). These model parameters are kept constant throughout the entire frequency range. Since the inductance is a function of the device geometry and the material properties. For simplicity, it can be assumed that the geometry is not a function of frequency. If the inductance is fitted to a constant, then the material properties are also constrained to be constant. For our case, as it can be seen by examining figure 2, the fit of the Bode plot is tolerable. However, the results of the fit cannot completely explain the variations of  $Z'$  and  $Z''$  with  $\omega$  (Figure 3).

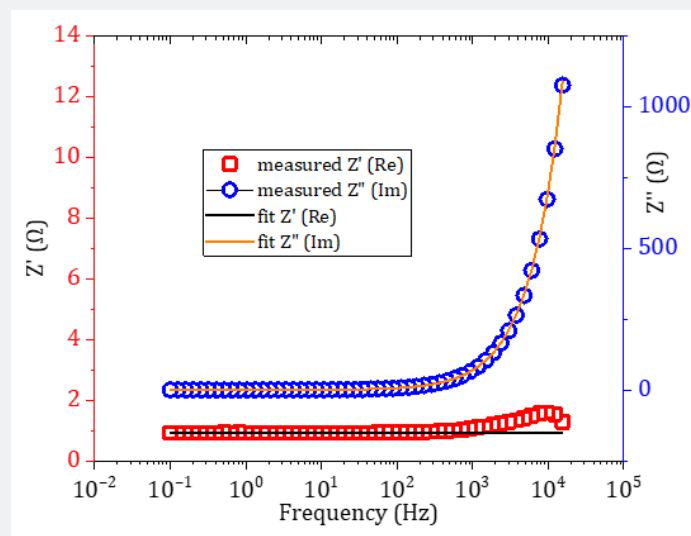


**Figure 3:** Real and imaginary parts of impedance. Experimental data is shown in points. The calculated curve is shown with continuous line. Here, the model used to fit the experimental data contains an inductor and two resistors connected in series.

It can be seen in figure 3 that the imaginary part is reasonably well described by the fit, however the observed real part is different from the calculated value at frequencies above 100 Hz. The fitting algorithm attempts to assign a fixed value for  $Z'$  throughout the entire frequency range. The observed  $Z'$  value is nearly constant with frequency through three orders of magnitude starting from 0.1 Hz, therefore the low frequency contribution to  $Z'$  outweighs the higher frequency discontinuity in the calculation of the overall  $Z'$  value. Since the reactance ( $Z''$ ) is up to three orders of magnitude higher than  $Z'$  this difference is not observed by the simple examination of the Bode plot.

An alternative approach is to use equations (6) and (7) to extract directly  $\mu'$  and  $\mu''$  from  $Z''$  and  $Z'$  respectively. Then the obtained relative effective permeability becomes a complex function of frequency. The main disadvantage is that any errors in the measurement of impedance are directly transmitted to the material properties. If data is extracted, rather than fitted,  $\mu'$  is observed on average between 978 and 993. Since the maximum current amplitude available in galvanostatic mode was only 0.5 mA the signal to noise ratio is rather small. Also,  $\mu''$  takes non-physical values. Higher currents are available if working in potentiostatic mode. However, on that mode, data acquisition is restricted to

single frequency measurements and the applied voltage must be set up manually, for each frequency, in order to maintain constant current amplitude. With the manually controlled potential difference method we were able to measure the impedance and permeability between 100 Hz and 1000 Hz for an applied current of 7 mA. This corresponds to an amplitude of the applied H field of

approximately 11.2 A/m. With this setup the measured effective real permeability ( $\mu'$ ) is observed between 993 and 1020. The corresponding imaginary part ( $\mu''$ ) is observed between  $\mu'' \approx 17$  at 100 Hz and  $\mu'' \approx 20$  at 1000 Hz. The results obtained by both fitting and extracting  $\mu'$  and  $\mu''$  are compared in figure 4.

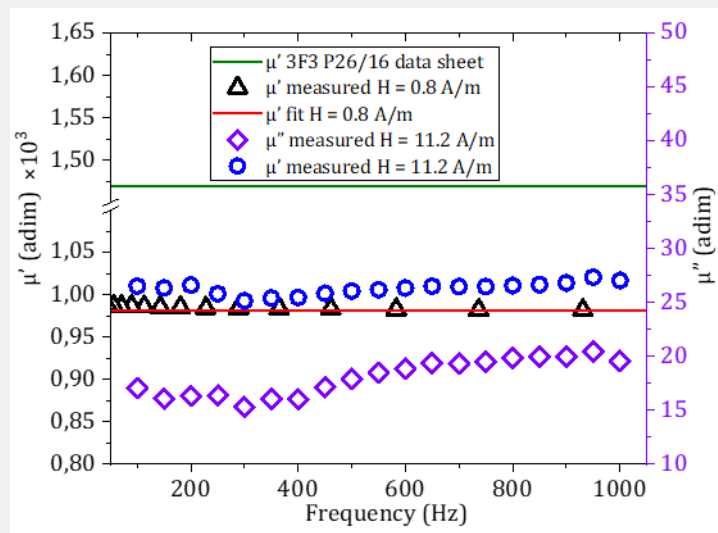


**Figure 4:** Expected, experimentally measured and fitted values for the real, respectively imaginary part of the effective magnetic permeability for 3F3. Fitted and expected curves are shown with continuous lines.

The parasitic capacity of the system was ignored at the frequency interval (100 Hz - 1 kHz) of the direct extraction experiment. At those frequencies, the corresponding reactive capacitance would be in the order of tens of megaohms (MΩ) while the impedance of the inductor is lower than 75 Ω. The observed  $\mu'$  remains below the expected value. It is inferred that the main cause for the observed decreased value of  $\mu'$  is the formation of some air gap due to the imperfect alignment of the core halves.

The variation of the magnetic induction (B) as a function of the applied magnetic field H was investigated on the same instrument. The measurements were carried out at a fixed frequency of 10 Hz in potentiostatic mode by varying the amplitude of the applied sinusoidal voltage between 7 mV and 500 mV. Thus, the peak H field reached approximately 850 A/m. According to the material data sheet this should be sufficient for observing the saturation of the magnetic induction. B(H) hysteresis was thus evidenced with little requirements for signal processing. The same coil is used both for generating the external magnetic field H and for recording the corresponding variation of magnetic inductance, B. When an inductor is subjected to the variation of a magnetic field a voltage is developed at the terminals of this inductor according to Faraday's law. The polarity of this voltage is determined according to Lenz's law. The time varying magnetic field could be generated by the induc-

tor itself. Then the generated voltage is the counter-electromagnetic force ( $\varepsilon$ ). The current that is established through the circuit is then given by equation (8) where U is the applied voltage and  $R_L$  is the ohmic resistance of the inductor, N is the number of turns and  $\Phi$  is the magnetic flux. The internal resistance of the analysis instrument and the resistance of the contact are neglected.

$$i = \frac{U - \varepsilon}{R_L} = \frac{U(t) - N \frac{d\phi}{dt}}{R_L} \quad (8)$$

The value of the counter-electromotive force can be easily extracted from the values of the measured current and applied voltage, according to equation (9).

$$\varepsilon = N \frac{d\phi}{dt} = U - R_L i \quad (9)$$

The counter-electromotive force is proportional to the time derivative of the magnetic flux. Then the magnetic flux is proportional to the integral of the counter-electromotive force. The magnetic flux can be defined according to equation (10):

$$d\phi = dBS \quad (10)$$

Therefore, the flux density (magnetic induction) should also be proportional to the integral of  $\epsilon$ :

$$B = \frac{1}{NS} \int_{t=0}^t \epsilon dt \quad (11)$$

For ease of observation figure 5 shows the obtained B(H) plots on 3 applied voltages, 130 mV, 350 mV and 500 mV. The smaller voltage setting induces a current of 95 mA amplitude which produces a magnetic field with a peak intensity of approximately 150 A/m. At this field saturation is not yet observed. For the other two

presented plots saturation can clearly be observed (where the H filed amplitude becomes  $\approx 600$  A/m and respectively  $\approx 850$  A/m). It is also observed that the overall slope of the B(H) plot is reduced. This is in agreement with the typical behaviour of magnetic cores that present a gap [12-14]. This observation is also in agreement with our estimations of the relative effective permeability. The observed lowering of the remanent magnetization could also be an effect of the introduction of the air gap. Table 3 shows the expected (according to material specifications) and observed (determined from the examination of the B(H) hysteresis plot) magnetic properties. The observed saturation value of the magnetic polarisation is  $\approx 400$  mT, in good agreement with the data sheet value of 440 mT [10].

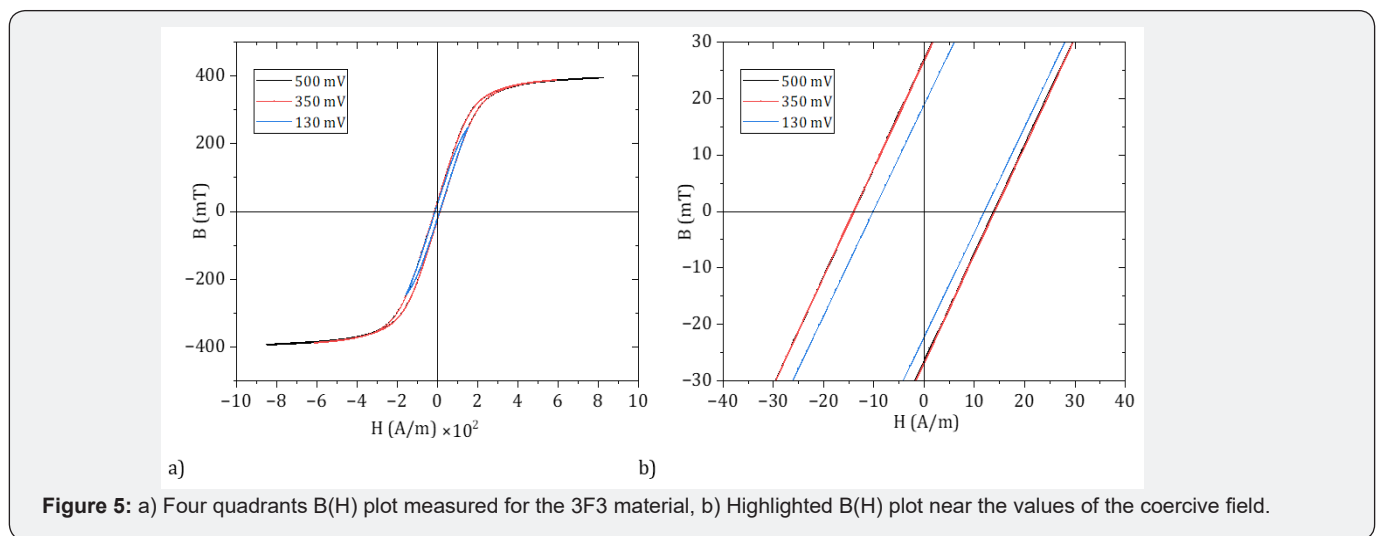


Figure 5: a) Four quadrants B(H) plot measured for the 3F3 material, b) Highlighted B(H) plot near the values of the coercive field.

Table 3: values of material characteristics.

Parameter	Unit	Measured	Data Sheet	Relative Error
magnetic polarisation at saturation value	mT	395	440	10.2 %
remanence	mT	27	150	-
coercive field	A/m	14	12.5 - 13	$\approx 12 - 8$ %

The observed coercive field nearly 14 A/m which is again in good agreement with the estimated coercive field according to the material specifications data sheet of 12.5-13 A/m [10]. It should be noted that the measurement of the coercive field is not yet accurate. It was observed that the applied magnetic field is not symmetrical to 0. The source of this asymmetry could be an experimental error caused by a very small residual DC applied at the same time with the AC signal. Indeed, the raw data indicated the presence of a DC current, about three orders of magnitude smaller than the peak AC current. The presence of the DC current could offset the AC signal and therefore the magnetic field is actually swept between  $(-H + \Delta H)$  and  $(+H + \Delta H)$  instead of the expected  $-H$  to  $+H$  range. The  $\Delta H$  value is subtracted from the raw data such that the coercive field should have the same magnitude on both

directions, i.e.,  $|-H_c| = |H_c|$ . Another possible explanation is related to calculation errors. The magnetic flux is proportional to the integral of the counter-electromotive force plus a constant, due to the integration operation itself. That constant is removed. However, the removal operation is another potential source of errors.

### Conclusion

The static and complex effective magnetic permeability, the saturation magnetic polarisation and the coercive field of the 3F3 material were determined from EIS measurements. The sample was available as a “pot” type inductor core. The measurements were carried out on a home-based inductor wound on the available sample. The measured material characteristics are relatively close to the expected ones according to the material data sheet, or

within the same order of magnitude. The measured static magnetic permeability is lower than the expected one by as much as 40 %. The difference could be caused by the sum of manufacturing tolerances and experimental errors. The accuracy in determining the imaginary part of the complex relative magnetic permeability is strongly dependent on the accuracy in determining the ohmic resistance of the coil. The imperfect overlap of the core parts could cause the development of an air gap which then lowers the observed value for the effective magnetic permeability. The observed shape of the B(H) hysteresis curve and the lowering of the magnetic remanence provide further support to the air gap hypothesis. Interestingly, the measured values for the coercive field and the magnetic flux density at saturation (for soft magnetic materials the magnetic flux density is almost identical to the magnetic polarisation) are close to the specified material characteristics. The estimated relative error for determining these two parameters is approximately 10 %. The measurements were not optimised for increasing the accuracy of the results but rather for exploiting the simplicity and availability of the EIS experimental setup.

Further testing is required by repeating the experiments on other soft magnetic materials. Sample preparation can compensate for the low voltage / low current typically employed by EIS. This may result in a reduction of the frequency band available for measurements, particularly at high frequencies.

### Acknowledgement

The research was possible through the Project “Development of a technological product – EOD active protection suit” code 119658, financed by the Ministry of Research, Innovation and Digitization through POC/163/1/3, AP1: CDI in supporting economic competitiveness and business development, Action 1.2.1, Project type - innovative technological project.

This work was financed by the Ministry of Research, Innovation and Digitization through the INOVADIT project, Programme 1 – Improvement of the national research and development system, Subprogramme 1.2 – Institutional performance – Projects for financing excellence in RDI, Contract no. 9PFE/2021.

### References

1. Barba A, Clausell C, Jarque JC, Nuño L (2020) Magnetic complex permeability (imaginary part) dependence on the microstructure of a Cu-doped Ni-Zn-polycrystalline sintered ferrite. *Ceramics International* 46(10): 14558-14566.
2. Vytautas D, Linas S (2006) Measurement of complex permeability of magnetic materials. *MATAVIMAI* 1(37): 27-32.
3. Riccardo T, Alessandra C (2014) A 1-kW Contactless Energy Transfer System Based on a Rotary Transformer for Sealing Rollers. *IEEE Transactions on Industrial Electronics* 61(11): 1-9.
4. Eun SL, Byeong GC (2021) Calculation Methodologies of Complex Permeability for Various Magnetic Materials. *Electronics* 10(2167): 1-9.
5. Lucian GP, Maria CP, Valentin I, Emil C, Cătălin DC (2019) Magnetic Properties of Manganese-Zinc Soft Ferrite Ceramic for High Frequency Applications. *Materials* 12(3173): 1-12.
6. Daniel M, Petr P (2012) A novel approach to measurement of permeability of magnetic fluids. *Electrical Review* 88(7b): 229-231.
7. Yabukami S, Ojima R, Yamaguchi M, Arai KI, Kikuchi S (2003) Highly sensitive permeability measurements obtained by electrical impedance. *Journal of magnetism and magnetic materials* 254: 111-114.
8. Denk F, Hofbauer T (2023) Determination of the Magnetic Intermediate Permeability of Special Materials Based on FEM-Simulation and Hall-Sensor Measurement. *Magnetism* 3(2): 169-179.
9. Barbara AL, Jan MVP (1982) Coil Winding/electrical Manufacturing Expo. Evaluation of Several Factors Affecting Inductance Measurements of Ferrite Components, Illinois – USA.
10. Ferroxcube Data Sheet, 3F3, (2008) Material Specification, <https://www.ferroxcube.com/upload/media/product/file/MDS/3f3.pdf>.
11. Ferroxcube, Soft Ferrites and Accessories Data Handbook (2013) <https://www.ferroxcube.com/en-global/download/download/11>.
12. International standard IEC 60404-3, Magnetic materials - Part 3: Methods of measurement of the magnetic properties of magnetic sheet and strip by means of a single sheet tester.
13. Epcos, Ferrites and accessories, Processing notes (2006) [https://www.dextermag.com/wp-content/uploads/2017/03/Dexter\\_EPCOS\\_Ferrite\\_Processing\\_Notes.pdf](https://www.dextermag.com/wp-content/uploads/2017/03/Dexter_EPCOS_Ferrite_Processing_Notes.pdf).
14. Zurek S, Encyclopedia Magnetica, Air gap, CC-BY-4.0, [https://www.encyclopedia-magnetica.pl/doku.php/air\\_gap](https://www.encyclopedia-magnetica.pl/doku.php/air_gap).



This work is licensed under Creative Commons Attribution 4.0 License  
DOI: [10.19080/JOJMS.2023.08.5557230](https://doi.org/10.19080/JOJMS.2023.08.5557230)

#### Your next submission with JuniperPublishers will reach you the below assets

- Quality Editorial service
- Swift Peer Review
- Reprints availability
- E-prints Service
- Manuscript Podcast for convenient understanding
- Global attainment for your research
- Manuscript accessibility in different formats  
**( Pdf, E-pub, Full Text, Audio )**
- Unceasing customer service

Track the below URL for one-step submission

<https://juniperpublishers.com/submit-manuscript.php>